Energy & Buildings 203 (2019) 109449

Contents lists available at ScienceDirect

Energy & Buildings

journal homepage: www.elsevier.com/locate/enbuild

Experimental investigation of energy and exergy performance of a direct evaporative cooler using a new pad type

S.A. Nada[a,*], A. Fouda[b], M.A. Mahmoud[a], H.F. Elattar[a]

[a] Mechanical Engineering Department, Faculty of Engineering at Benha, Benha University, 13512 Benha, Egypt
[b] Department of Mechanical Power Engineering, Faculty of Engineering, Mansoura University, 35516 El-Mansoura, Egypt

ARTICLE INFO

Article history:
Received 11 July 2019
Revised 30 August 2019
Accepted 22 September 2019
Available online 23 September 2019

Keywords:
Evaporative cooler
Bee-hive pad
Cooling capacity
Saturation efficiency
Exergy efficiency

ABSTRACT

In this paper a comprehensive experimental parametric study on the performance of a new evaporative cooling pad type made of cellulose papers in bee-hive structure is presented. Four different pad sizes of face area 0.335 × 0.390 m^2 and thicknesses 35, 70, 105, and 140 mm are examined. The tests are carried out in a wind tunnel adapted with the evaporative cooling system. Experiments are conducted to evaluate the cooling pad performance parameters: air temperature drop, air humidity ratio raise, cooling capacity, water evaporation rate, saturation efficiency, pressure drop, energy efficiency, energy efficiency ratio, exergy efficiency and overall exergy efficiency. The effects of the cooling pad thickness and the operating conditions including air velocity, inlet air temperature, water flow rate, water temperature and cooling pad thickness on the performance parameters are investigated. The results show that, the saturation efficiency, exergy efficiency and overall exergy efficiency of the proposed pad enhance with increasing the pad thickness and water flow rate and their highest obtained values are 84%, 92% and 74%, respectively. The maximum pressure drop, temperature drop and cooling capacity obtained for this pad are 46 Pa, 18 °C and 6.26 kW, respectively. Moreover, the highest energy efficiency ratio is 281 obtained at 2 m/s air velocity. Finally, new dimensionless experimental correlations for predicting the system performance parameters in terms of various operating conditions and system size are presented.

1. Introduction

Electricity consumption of buildings sector represents 32% of the whole world consumption as indicated by the International Energy Agency [1]. Recently, buildings sector was considered the biggest consumer of electricity. Conventional air-conditioning using vapor compression system consumes about 20% of the total electricity consumed in buildings all over the world. Evaporative cooler can be considered one of the effective solutions of the electricity consumptions in buildings [2]. For example, in a regular 200 m^2 house, the common energy usage of evaporative cooler is as little as 250.0 kWh compared to 850.0 kWh for traditional air-conditioner units (i.e. 75% power saving) [2-3]. By tracking the energy consumption of evaporative cooler in a small commercial building, it's observed significant energy savings and improvement in thermal comfort as compared with conventional air-conditioning systems [4]. In evaporator cooler air and water passes in cross flow configuration through a porous wetted medium/pad and comes in contact causing water evaporation and air cooling. The cooling pad is kept wet by continuous feed of spraying water over it. Evaporative cooler is most appropriate for hot and dry regions as in most of the Middle East cities.

Some studies integrate the idea of evaporative cooler with cooling of condensers of air condition units in a trial to reduce the electrical consumptions. Yu and Chan [5] reported that the performance of the air-conditioning systems can be improved by using evaporative pre-cooling to drop down the temperature of the air that pass on the air-cooled condenser. Hao et al. [6] developed a mathematical model to evaluate the energy saving in evaporative air-cooled chillers (EACC) and reported that there is an optimal thickness of the cooling pad that gives maximum energy saving. Others investigators [7–9] conducted experimental works that integrated an evaporative cooler with small air-conditioning condenser (split-unit). It was shown that the reduction in power consumption and the improvement in the COP of the AC split-unit can reach 10–30% and 10–50%, respectively by this integration.

Several studies were conducted to investigate the performance of different cooling pads material to examine their suitability for

Abbreviations: EER, energy efficiency ratio; w.r.t, with respect to.

* Corresponding author at: Mechanical Engineering Department, Faculty of Engineering at Benha, Benha University, Benha, Egypt.
E-mail addresses: sameh.nada@ejust.edu.eg (S.A. Nada), eng_alifouda@mans.edu.eg (A. Fouda), mohamed.ashraf@bhit.bu.edu.eg (M.A. Mahmoud), hassan.alattar@bhit.by.edu.eg (H.F. Elattar).

https://doi.org/10.1016/j.enbuild.2019.109449
0378-7788/

Nomenclature

c_p	Constant pressure specific heat [kJ. Kg^{-1}.K^{-1}]
ex	specific exergy [kJ.kg-1]
ex^{ch}	chemical specific exergy [kJ.kg-1]
$\dot{E}x$	rate of exergy destruction [kW]
g	standard gravitational acceleration [m.s-2
$g^o_{f,w(l)}$	Gibbs function of formation [kJ.kg-1]
HP	circulating pump head [m]
h	specific enthalpy [kJ.kg-1]
M	Molar mass [kg.kmol-1]
$\dot{m}$	mass flow rate [kg.s-1]
$\dot{Q}_c$	sensible cooling capacity [kW]
ν	mean velocity [m.s-1]
R	gas constant [kJ. Kg-1.K-1]
s	specific entropy [kJ. Kg-1.K-1]
$\dot{S}$	rate of entropy [kJ.K-1]
T	Temperature [oC]
$\dot{V}_{air}$	air volume flow rate [m3.s-1]
$\dot{W}_{fan}$	fan power consumption [kW]
$\dot{W}_{pump}$	pump power consumption [kW]
y	mole fraction of the gas phase
z	Elevation [m]

Greek symbols

δ	evaporative pad thickness, mm
ΔP	pressure drop of evaporative cooling pad [Pa]
Δt	temperature drop of evaporative cooling pad [oC]
$\Delta\omega$	Humidity ratio increase of evaporative cooling pad [gv.kga-1]
η	saturation efficiency
ηen	energy efficiency
ηex	exergy efficiency
ηex,overall	overall exergy efficiency
ρ	Density [kg.m-3]
ω	Air specific humidity ratio (mass basis) [kgv.kga-1]
$\tilde{\omega}$	Air specific humidity ratio (molar basis) [kmolv.kmola-1]
χ	arbitrary variable

Subscripts

0	dead state condition
1	inlet air flow
2	outlet air flow
a	dry air
dest	destruction
evap	evaporated
g	gas
gen	generation
i	Arbitrary parameter for inlet/outlet air flow
l	liquid
v	water vapor
w	water
wb	wet-bulb

evaporative cooler. Al-Sulaiman [10] experimentally studied the performance of three evaporative natural fibers cooling pads (Palm, Jute and Luffa fibers) and reported that their highest cooling efficiencies at 2.4 m/s air velocity are 62.10%, 55.10%, and 38.90%. Koca et al. [11] constructed a test facility for evaporative cooling-pads and verified that the pad cooling efficiency and air pressure drop depend mainly on the air velocity and pad thickness. Kovačević and Sourbron [12] presented numerical model to study heat and mass transfer in a novel design of metallic-compact direct evaporative cooler. It was reported that the highest effectiveness was obtained for evaporative pad thickness of 90 mm at low air velocities. Liao and Chiu [13] constructed a wind tunnel for testing different evaporative cooling pads of fine and coarse mesh and they noticed that the coarse fabric type has better performance. Rawangkul et al. [14] tested the performance of a direct-evaporative cooling pad made from coconut coir of two different configurations. They concluded that coconut coir has good characteristics to be used as a wetted medium in evaporative cooling systems. Gunhan et al. [15] conducted an experimental study to test different porous materials (pumice stones, volcanic tuff and greenhouse shading net) to be used as alternative to CELdek cooling pad which was commercially used. The results verified that the volcanic tuff pads can be considered as efficient alternatives of CELdek pads at 0.60 m/s air velocity. Jain and Hindoliya [16] conducted an experimental study to compare the performance of coconut fibers and palash fibers with the aspen and khus pads. It was observed that the pad efficiency of palash fibers is 13.20% and 26.30% more than aspen and khus pads, respectively, while the efficiency of the coconut fibers is about 8.2% more than that of khus.

Other studies were conducted for different geometric constructions of cooling pads materials. Beshkani and Hosseini [17] carried out a mathematical analysis on the behavior of corrugated papers (rigid media) cooling pad using finite difference technique. It was verified that increasing the pad thickness increases the cooling pad efficiency and the air pressure drop. Dai and Sumathy [18] solved the governing equations for cross-flow direct evaporative cooling combined with honeycomb papers of uniform channels spacing as a cooling pad. They reported that the efficiency of the cooling pad can be improved by optimizing the operating conditions and geometric dimensions including air and water mass flow rates and pad thickness. Wu et al. [19,20] conducted a numerical investigation on direct-evaporative coolers using honeycomb papers as a cooling pad. It was reported that the efficiency of the cooling pad increases with decreasing air velocity and increasing cooling pad thickness. Malli et al. [21] conducted an experimental investigation on the behavior of evaporative cooling pads made of cellulose corrugated papers of different thickness. They proved that increasing the air flow velocity and the thickness of the cooling pads increases the air pressure drop and reduces the cooling efficiency. Trade-off between air pressure drop and the evaporator efficiency should be considered. Dhamneya et al. [22] presented a comparative analysis on square, triangle, pentagon, octagonal and hexagonal cooling pads configurations in order to find the configuration of high wetted contact areas for the air. It was observed that the triangle configuration has the highest cooling efficiency. Moreover, the effects of the operating conditions including air velocity, air temperature, water flow rate and water temperature on the water evaporation rate in humidification section of HDH system were recently conducted [23–27].

Other investigations were conducted to evaluate the performance of evaporative cooling pads based on energy-exergy analysis. For energy saving, Doğramacı et al. [28] experimentally investigated the performance of an evaporative cooler using eucalyptus fiber pads. They reported that the maximum temperature drop can reache 11.3 °C with a maximum cooling efficiency of 71% at 0.1 m/s air velocity. Laknizi [29] studied the performance of evaporative cooling pads and the energy saving under different weather conditions of six cities in Morocco. It was noticed that the water consumption rate and the cooling capacity increases and the COP decreases with increasing the air velocity and the pad thickness. Kanoglu et al. [30] carried out a parametric study on the heating and humidification process of air conditioning system to prove that the operating conditions have a considerable effect on the exergy change. Santos et al. [31] presented an analytical investigation on

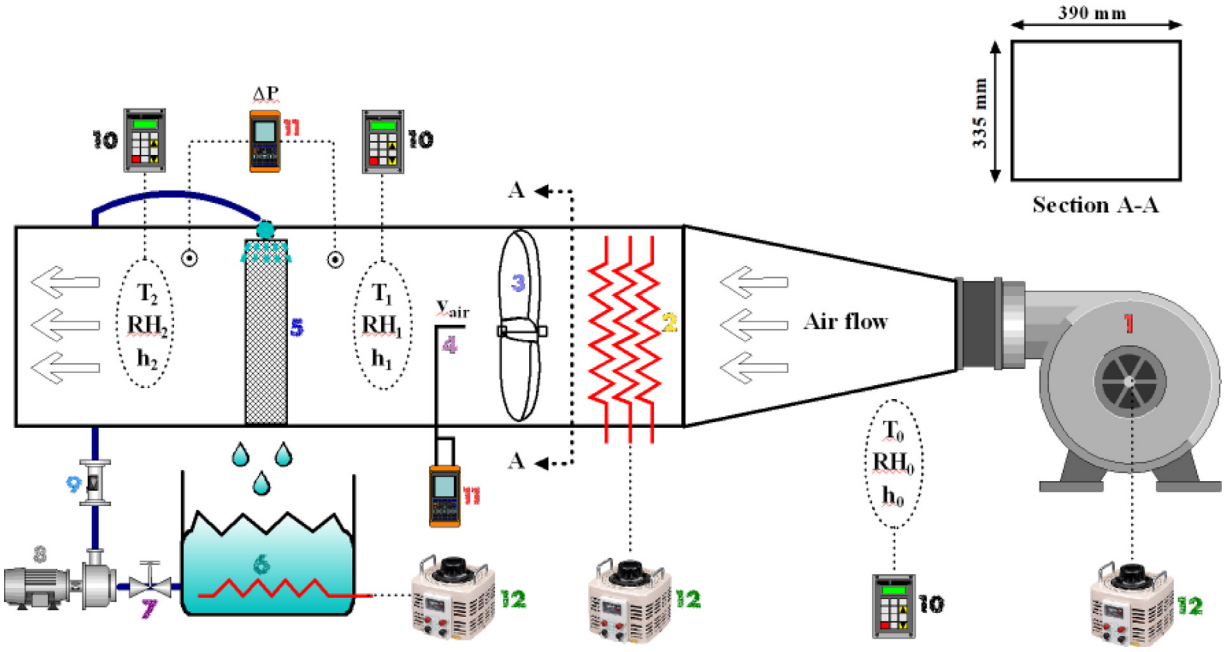

Fig. 1. Schematic diagram of experimental setup.

the evaporative cooler from energy-exergy viewpoints. They confirmed that the best operating conditions for getting optimum energy efficiency don't match with the conditions of thermal comfort. Martínez et al. [1] conducted and experimental investigation on the performance of evaporative pad (plastic mesh) from energy and exergy standpoints. The results showed that the maximum saturation efficiency and pressure drop for that pad type are 80% and 17 Pa, respectively.

In the present work the performance of a new cooling pad made from corrugated cellulose papers in opposite arrangement with a "bee-hive" construction is experimentally investigated. The manufacturer/supplier of the pad is Wadi Group Company in Egypt, under the trade name of "Tabreed" [32]. The effects of operating conditions and geometric parameters (frontal air velocity, air inlet temperature, spray water flow rate, spray water temperature, cooling pad thickness) on the system performance parameters (air temperature drop and humidity rise, pressure drop, saturation efficiency, evaporated water rate, sensible cooling capacity, energy efficiency ratio, energy efficiency, exergy efficiency and overall exergy efficiency) are investigated and quantified based on energy and exergy standpoints analysis. New empirical correlations for the performance parameters are deduced from the huge experimental data in terms of the operating conditions and design parameters.

2. Experimental methodology

2.1. Experimental setup and physical components

The experimental setup is designed, constructed and validated to carry out comprehensive experiments for a wide range of operating and design conditions (air velocity, inlet air temperature, water flow rate and water inlet temperature, and pad thickness) in order to investigate the performance of the proposed cooling pad in details. To accurately evaluate and characterize the behavior and performance, the cooling pads were tested in a wind tunnel system (See Fig. 1) under steady state subsonic conditions. The wind tunnel consists of different sections including air fan/blower, electric heaters for air heating, air mixer, and evaporative cooler including the cooling pad and water circuit. The wind tunnel is an open circuit, rectangular duct of 390 mm (width) × 335 mm (height) cross-section and overall length of 3000 mm. The tunnel walls are 0.8 mm thick galvanized sheet steel thermally insulated by 25-mm thick glass wool. The air supply section consists of blower, flexible connection, and diverging section. The air blower (735 W, 220 V and 50 HZ) is a variable speed blower with 100 mm x 120 mm discharge cross section. The speed of the blower is controlled using a voltage regulator to change the air flow rate by changing the input voltage. The air is then passes around three electric heaters of 3 kW each staggered arranged in the wind tunnel to occupy the entire cross section area of the tunnel. A voltage regulator is used to control the power input to the heaters in order to regulate and obtain the required air temperature needed for each experiment. The air is then flow through an air mixer to obtain a uniform air temperature along the cross section area of the air duct. The air is finally passes through the evaporative cooling pad section to cool it.

The direct evaporative cooling system is equipped with water supply unit and consists of re-circulating water pump, water tank, electric water heater, spray water distributer, evaporative cooling pads with bee-hive structure and piping and control valves as shown in Fig. 1. The working principle is that the evaporative cooling pad is wetted continuously by spraying water vertically onto the upper edge of the cooling pad and the air passes horizontally in cross-flow arrangement with the water. As a result, water evaporates with the air when it passes through the pad. This water evaporation absorbs its heat of evaporation from the air and causes a reduction in the air temperature. Finally, the air exits from the humidifier at a low temperature and high humidity (i.e. it's cooled and humidified). In the water supply unit, the re-circulating water pump is 380 V, 50 Hz, and 10 liter/min capacity. The water tank contains a serpentine-shape water electrical heater (1500 W) connected to a voltage regulator to control the feed water temperature. The spray water distributer is fabricated from a steel pipe of 1-inch diameter with 13-holes and with spacing of 30 mm and overall length of 500 mm.

Four evaporative cooling pads of type Tabreed 45/45 angle [32] and thicknesses 35, 70, 105 and 140 mm were tested. The

Table 1
Technical specifications of measuring instrumentations.

Measuring instruments	Measured parameters	Range	Accuracy	Resolution
Hygro-thermometer (HTC-1)	Temperature Relative humidity	−50 to +70 °C 10% to 99% RH	± 1 °C ± 5% RH	± 0.1 °C ± 1% RH
Hygro-thermometer (SH-109)	Temperature (ambient) Relative humidity (ambient)	−10 to 50 °C indoor −50 to +70 outdoor 20% to 99% RH	± 1 °C ± 5% RH	± 0.1 °C ± 1%R H
Temperature sensor (PT100) & digital thermometer (TC4Y)	Temperature	−50 to 400 °C	± 1 °C	± 0.1 °C
Digital differential pressure manometer 0.5 PSI (HD755)	Pressure drop (cooling pads)	0 – 0.5 Psi	±0.3%	0.001 Psi
Pitot tube anemometer & manometer (HD-350)	Measures Air Velocity/Airflow in difficult-to-reach or tight locations	1 to 80.00 m/sec	±1%	0.01

pads section consist of corrugated sheets of cellulose 0.7 mm thick grouped in an opposite sequential arrangement with a "bee-hive" structure to generate the flow of air inside the cells. The pad configuration and full dimensions are illustrated in Fig. 2. The material of these sheets has an excellent ability to water abortion and chemically treated using an odorless substance to achieve exceptional wetting properties [32].

2.2. Measuring instrumentation devices

The experimental setup is equipped with the measuring instrumentation devices needed to measure and record the physical parameters that are necessary for the data analysis including temperatures, air humidity, pressure drop, electrical power, air velocity and water flow rate. The measuring instruments used in this study are hygro-thermometers, digital thermometer, digital differential pressure manometer and Pitot tube anemometer & manometer. Three hygro-thermometers were installed in the setup to measure the relative humilities and temperatures at different locations in the tunnel section as shown in Fig. 1. Two hygro-thermometers are located at the inlet and outlet of the evaporative cooler, while the third one (SH-109) is used to measure the ambient air condition in the laboratory. PT100 temperature sensor was connected with a digital thermometer (model TC4Y) to measure the temperatures at the inlet of the evaporative pad. A digital differential pressure manometer (0.5 PSI, HD755) is used to measure the air pressure drop across the evaporative pad. Pitot tube anemometer & manometer (HD-350) are used to measures the air velocity and airflow rate in the air duct. The detailed specifications of the measuring instruments are given Table 1.

Table 2
Studied parameters and their values.

Studied parameter	Value
Frontal air velocity, v_{air}	1, 1.5, 2, 2.5 and 3 m/s
Cooling pad thickness, δ	35, 70, 105 and 104 mm
Air inlet temperature, T_1	30, 35, 40, 45 and 50 °C
Spray water flow rate, $\dot{m}_w$	0.0465, 0.0952, 0.1176 and 0.1667 kg/s
Spray water temperature, T_w	25, 30, 35 and 40 °C

2.3. Experimental procedure and measurements

Eighty two experiments were carried out to test the cooling pads for different pad thicknesses, air velocities, inlet air temperatures, water flow rates and temperatures ranges as given in Table 2. Before recording any test, steady state conditions should be maintained. To ensure maintaining the steady state condition, the experiment was turned on a long period, at least 30–40 min, before taking the measurements until ensuring that the senor readings are constants without significant fluctuations and within the accuracy of the instrumentations.

For the validation of the procedure and accuracy of the present experimental work, several preliminary experiments have been carried out on widely used evaporative cooling pad (CELdek) made of cellulose media by Munters company as a reference material for

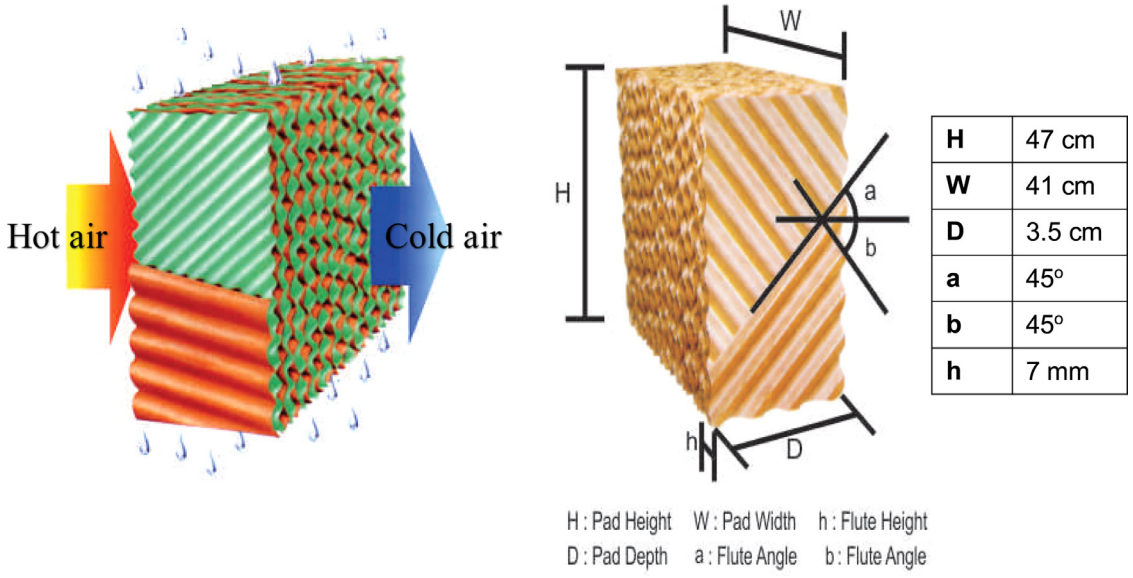

H	47 cm
W	41 cm
D	3.5 cm
a	45°
b	45°
h	7 mm

Fig. 2. Configuration and full dimensions of utilized model bee-hive cellulosic pad.

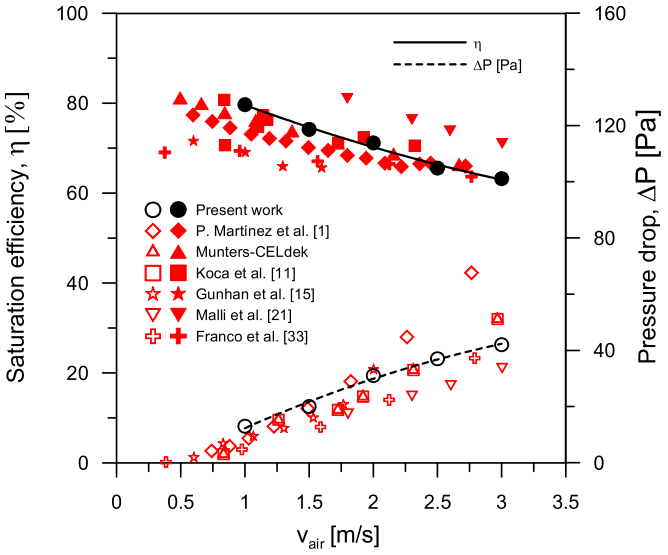

Fig. 3. Validation of the experimental test method (comparison of the present experimental results with other previously reported results).

comparisons. The validation tests were conducted on cooling pad of 100 mm thickness at a wide range of air velocity and the saturation efficiency and air pressure drop were calculated for each experiment. The obtained data was checked and compared with the data collected from different researchers [11,15,21,33]. As shown in Fig. 3, the results obtained from the present study have approximately the same values presented by other authors for the same cooling pad.

2.4. Mathematical analysis

The evaporative cooling process can be analyzed and characterized by conducting mass, momentum, energy and exergy balances for the cooling pad section as given below:

$$\dot{m}_{a,1} = \dot{m}_{a,2} \tag{1}$$

$$\dot{m}_{a,1}\,\omega_1 + \dot{m}_{w,evap} = \dot{m}_{a,2}\omega_2 \tag{2}$$

$$\dot{m}_{a,1}\,h_1 + \dot{m}_w\,h_w = \dot{m}_{a,2}h_2 \tag{3}$$

Moreover, the exergy balance was presented by Dincer and Rosen [34] and Moran et al. [35]:

$$\dot{m}_{a,1}\,(ex)_1 + \dot{m}_w\,(ex)_w - \dot{m}_{a,2}\,(ex)_2 - (\dot{E}x)_{dest} = 0 \tag{4}$$

$$(ex)_i = (h_{a,i} - h_{a,0}) - T_0(s_{a,i} - s_{a,0}) + \omega_i[(h_{v,i} - h_{v,0}) - T_0(s_{v,i} - s_{v,0})] + v_i^2/2 + gz_i + (ex)_{a,i}^{ch} \tag{5}$$

$$(ex)_{a,i}^{ch} = R_a T_0\left[(1+\tilde{\omega}_i)\ln\left(\frac{1+\tilde{\omega}_0}{1+\tilde{\omega}_i}\right) + \tilde{\omega}_i \ln\frac{\tilde{\omega}_i}{\tilde{\omega}_0}\right] \tag{6}$$

Where, $\tilde{\omega}_i = \frac{M_a}{M_v}\omega_i = 1.608\omega_i$, $\tilde{\omega}_0 = \frac{M_a}{M_v}\omega_0 = 1.608\omega_0$

$$(ex)_w = (h_w - h_0) - T_0(s_w - s_0) + v_w^2/2 + gz_w + (ex)_w^{ch} \tag{7}$$

$$(ex)_w^{ch} = g_{f,w(l)}^o - g_{f,w(g)}^o + R_w T_0 \ln\left(\frac{1}{y_{v,0}}\right) \tag{8}$$

$$(\dot{E}x)_{dest} = T_0\dot{S}_{gen} = T_0(\dot{m}_{a,2}s_2 - \dot{m}_{a,1}s_1 - \dot{m}_{w,evap}s_w) \tag{9}$$

The evaporative cooling efficiency (saturation efficiency) can be calculated by Eq. (10) [36]:

$$\eta = \frac{(T_1 - T_2)}{(T_1 - T_{wb,1})} \tag{10}$$

The energy efficiency, η_{en} is defined as the ratio of outgoing stream energy to the sum of the incoming stream energies as provided by Kanoglu et al. [30]:

$$\eta_{en} = \frac{\dot{m}_{a,2}h_2}{\dot{m}_{a,1}h_1 + \dot{m}_{w,evap}h_w} \tag{11}$$

The exergy and overall exergy efficiencies, η_{ex} & $\eta_{ex,overall}$, can be obtained based on Martínez et al. [1] as follows:

$$\eta_{ex} = \frac{\dot{m}_{a,2}(ex)_2}{\dot{m}_{a,1}(ex)_1 + \dot{m}_{w,evap}(ex)_w} = 1 - \frac{(\dot{E}x)_{dest}}{(\dot{E}x)_{in}} \tag{12}$$

where,

$$(\dot{E}x)_{in} = \dot{m}_{a,1}(ex)_1 + \dot{m}_{w,evap}(ex)_w$$

$$\eta_{ex,overall} = \frac{\dot{m}_{a,2}(ex)_2}{\dot{m}_{a,1}(ex)_1 + \dot{m}_{w,evap}(ex)_w + \dot{W}_{fan} + \dot{W}_{pump}} \tag{13}$$

Where, $\dot{W}_{fan}$ and $\dot{W}_{pump}$ are the fan and pump power consumptions, calculated according to the air and water flow rates [6] as follows:

$$\dot{W}_{fan} = \frac{\dot{V}_{air}\Delta P}{\eta_{fan}} \tag{14}$$

$$\dot{W}_{pump} = \frac{\dot{m}_w \rho_w H_P g}{\eta_{pump}} \tag{15}$$

η_{fan} and η_{pump} are the fan and circulating pump efficiencies, respectively, which are taken as 80% in this work [6].

The sensible cooling capacity is a vital parameter for analysis of cooling pad performance as given by:

$$\dot{Q}_c = \dot{m}_a c_p (T_1 - T_2) \tag{16}$$

The performance analysis was also performed using the energy efficiency ratio (*EER*), which is the ratio of sensible cooling capacity ($\dot{Q}_c$) to total electric power consumption of the fan ($\dot{W}_{fan}$) and water pump ($\dot{W}_{pump}$) [37] and presented as:

$$EER = \frac{\dot{Q}_c}{\dot{W}_{fan} + \dot{W}_{pump}} \tag{17}$$

The evaporative cooler performance is investigated by solving the former equations using EES (Engineering Equation Solver software); commercial version (6.883–3D). All air and water properties are obtained from EES data base at the measured temperature and humidity.

It is essential to determine the experimental error of the measurements and calculated variables. Uncertainty analysis can be applied by using the formula of Mofatt [38] and Taylor [39] in terms of the source error (see Table 1) of the variables measured in the experimental tests (i.e. temperature, relative humidity, air velocity, ...etc.). The equations from (1) to (17) can be put in the form of $Y = f(X_1, X_2, X_3, \ldots, X_n)$ where Y is the required parameter and $(X_1, X_2, X_3, \ldots, X_n)$ are the set of measured parameters.

The experimental uncertainty can be obtained by Eq. (18):

$$\delta Y = \sqrt{\left(\frac{\partial Y}{\partial X_1}\delta X_1\right)^2 + \left(\frac{\partial Y}{\partial X_2}\delta X_2\right)^2 + \cdots\cdots + \left(\frac{\partial Y}{\partial X_N}\delta X_n\right)^2} \tag{18}$$

Where $\delta Y$is the uncertainty of the required parameter and δX_1, δX_2, ...δX_n are the uncertainties of the measured variables and $\frac{\partial Y}{\partial X_i}$ is numerically calculated. The minimum and maximum overall uncertainty for the calculated parameters is given in Table 3.

Table 3
Overall uncertainty of calculated parameters.

Parameter	$\delta\eta$	$\delta \dot{m}_{w,\,evap}$	$\delta \dot{Q}_c$	δEER	$\delta\eta_{ex}$	$\delta\eta_{ex,\,overall}$
Min. uncertainty	1.5%	2.3%	2.5%	1.6%	4.6%	4.9%
Max. uncertainty	2.9%	11.9%	13.2%	8.6%	9.3%	9%

3. Results and discussion

The obtained results show that the performance of the tested cooling pads depends on the operating conditions: air flow rate, air temperature, water flow rate and water temperature as well as on the thickness of the cooling pad. Efficient evaporative cooling pads should maximize the air temperature drop and minimize the water consumption rate and air pressure drop. The air temperature drop, air pressure drop and water consumption rate for a specific size/capacity of the evaporative cooler depend on the operating conditions (air flow rate, air temperature, and water flow rate and water temperature). Unfortunately, their dependences are not all in the same required direction. Thus, determining the operating condition that gives the best system performance needs an optimization and dimensionless parameters that measure the performances of the cooling pads. These parameters as defined in the literature and given in the present introduction section include saturation efficiency, energy efficiency, energy efficiency ratio, exergy efficiency and the overall exergy. At the same time, to increase the size/capacity of the evaporative cooling system, the bad thickness, air flow rates and water flow rate should be increased to satisfy the increase in the cooling capacity. The operating conditions that give the best performances of the system may vary from a system to another according to the system size and capacity.

In the present work a comprehensive parametric study of the performances of the proposed cooling pad sections are conducted at a wide range of the operating conditions and system sizes. The performance of the system was evaluated by air temperature drop, air humidity ratio raise, cooling capacity, water evaporation rate, saturation efficiency, pressure drop, energy efficiency, energy efficiency ratio, exergy efficiency and overall exergy efficiency. The effects of the operating conditions and the system size parameters (air velocity, inlet air temperature, spray water flow rate, spray water temperature and cooling pad thickness) on each of the performance parameters are investigated in the following sections. This parametric study aims to determine the conditions that give

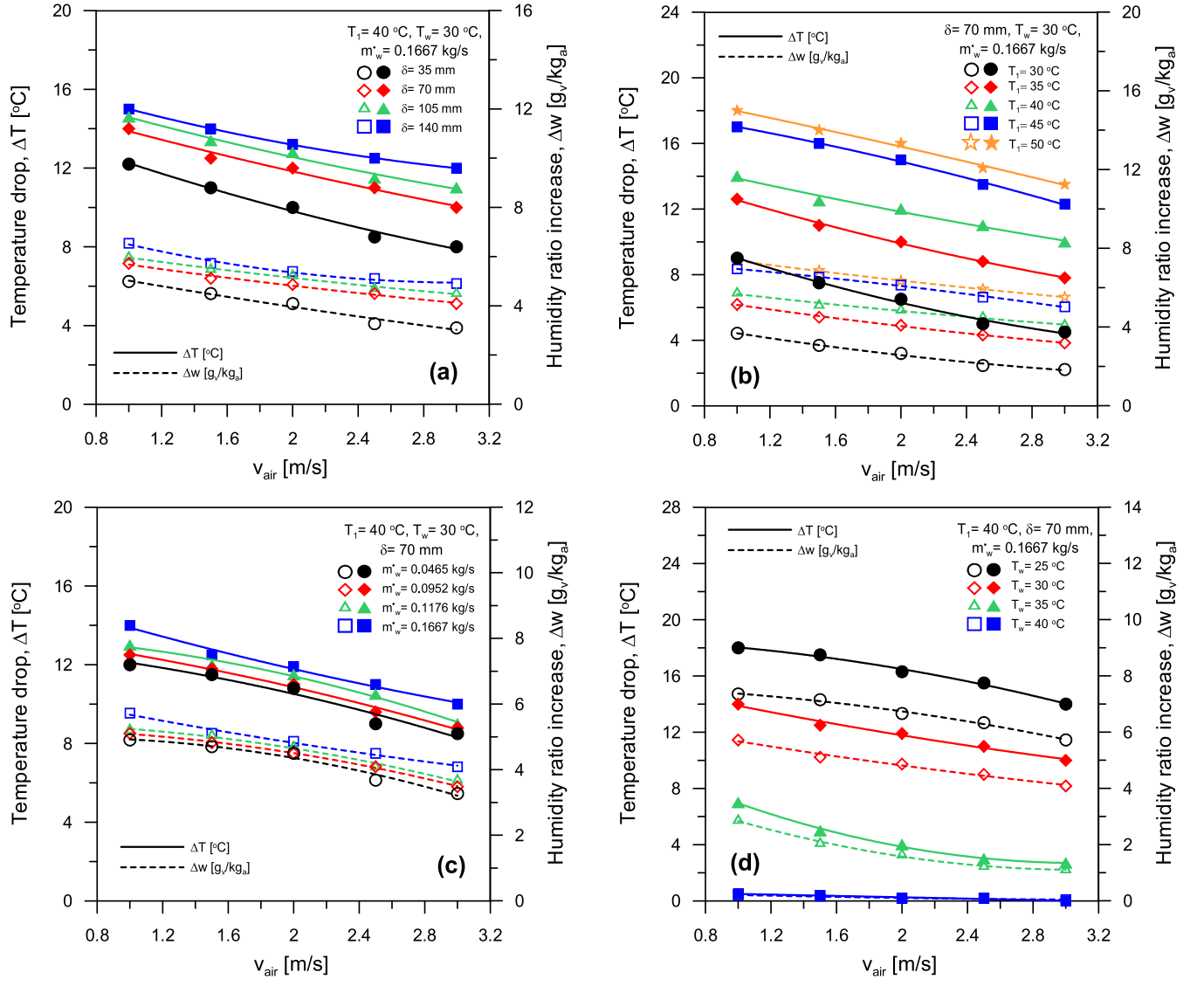

Fig. 4. Air temperature drop and humidity ratio increase across the cooling pad at different: (a) pad thickness, (b) air inlet temperature, (c) humidifier-water flow rate, (d) humidifier-water temperature.

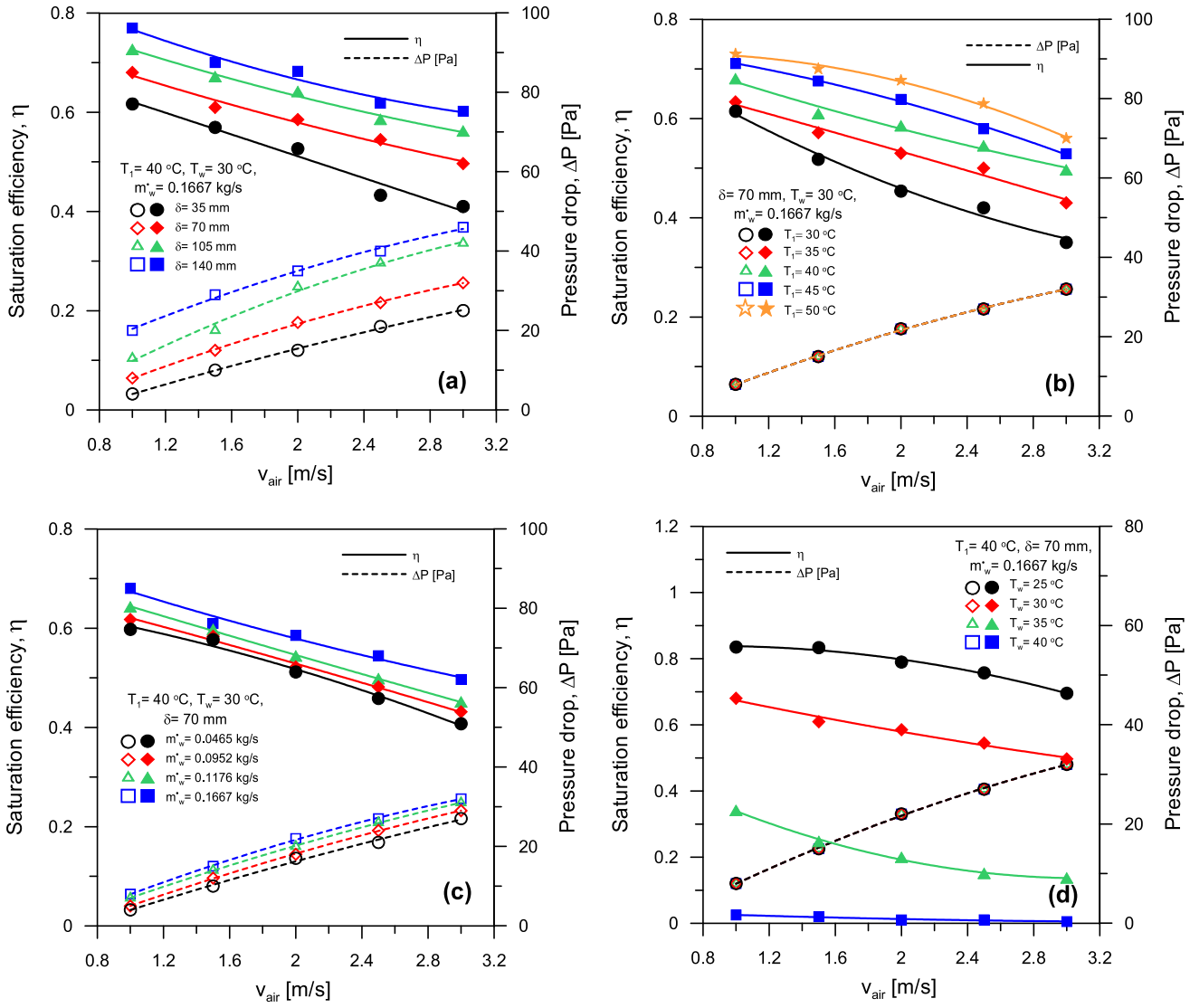

Fig. 5. Saturation efficiency and pressure drop across the cooling pad at different: (a) pad thickness, (b) air inlet temperature, (c) humidifier-water flow rate, (d) humidifier-water temperature.

optimum performance of the evaporative cooling using this type of cooling pad for different sizes. Finally, correlations that give the system performance parameters in terms of the operating conditions and the system size were proposed to be used in predicting the cooling pad performance for any operating conditions and system size.

3.1. Air temperature drop and humidity ratio increase

Fig. 4 shows the effect of air velocity, inlet air temperature, water flow rate, water temperature and pad thickness on the air temperature drop (ΔT) and humidity rise (Δw). The figure shows the decrease of ΔT and Δw with the increase of air velocity. This can be attributed to the decrease of the contact time between the air particles and the wetted pad with the increase of air velocity causing the reduction of the water evaporation rate which means the decrease of the air cooling potential. It worth to mention that increasing the air flow rate causes the increase of the mass transfer coefficient between the air and the wetted cooling pad and this leads to the increase of the water evaporation rate but according to the results shown in Fig. 4, this increase cannot compensate the decrease in the water evaporation rate resulted from the reduction of the contact time.

Fig. 4-a shows the variation of ΔT and Δw with cooling pad thickness at $T_1 = 40\,°C$, $T_w = 30\,°C$, $\dot{m}_w = 0.1667\,kg/s$ and a wide range of air velocity. The figure shows the increase of the temperature drop and the humidity of the air with the increase of the pad thickness. This can be attributed to the increase of the contact time between the air particles and the pad section which leads to the increase of the water evaporation rate and air temperature drop. The same results were obtained for different inlet air temperatures, water flow rates and water inlet temperatures. Also as shown in Fig. 4-a, the highest ΔT and Δw that can be obtained are 12.2, 14, 14.6 and 15 °C and 5, 5.7, 6 and 6.5 g_v/kg_a for pad thicknesses of 35, 70, 105 and 140 mm obtained at 1 m/s air velocity, i.e. ΔT and Δw increases by 23% and 30%, respectively with increasing the pad thickness from 35 mm to 140 mm.

Fig. 4-b demonstrates the effect of the air inlet temperature on the air temperature drop and humidity rise across the cooling pad section. As shown in the figure the air temperature drop and humidity rise increase with the increase of the air inlet temperature. This can be attributed to (i) the increase of the capacity of the air to hold more vapor with the increase of air temperature, and

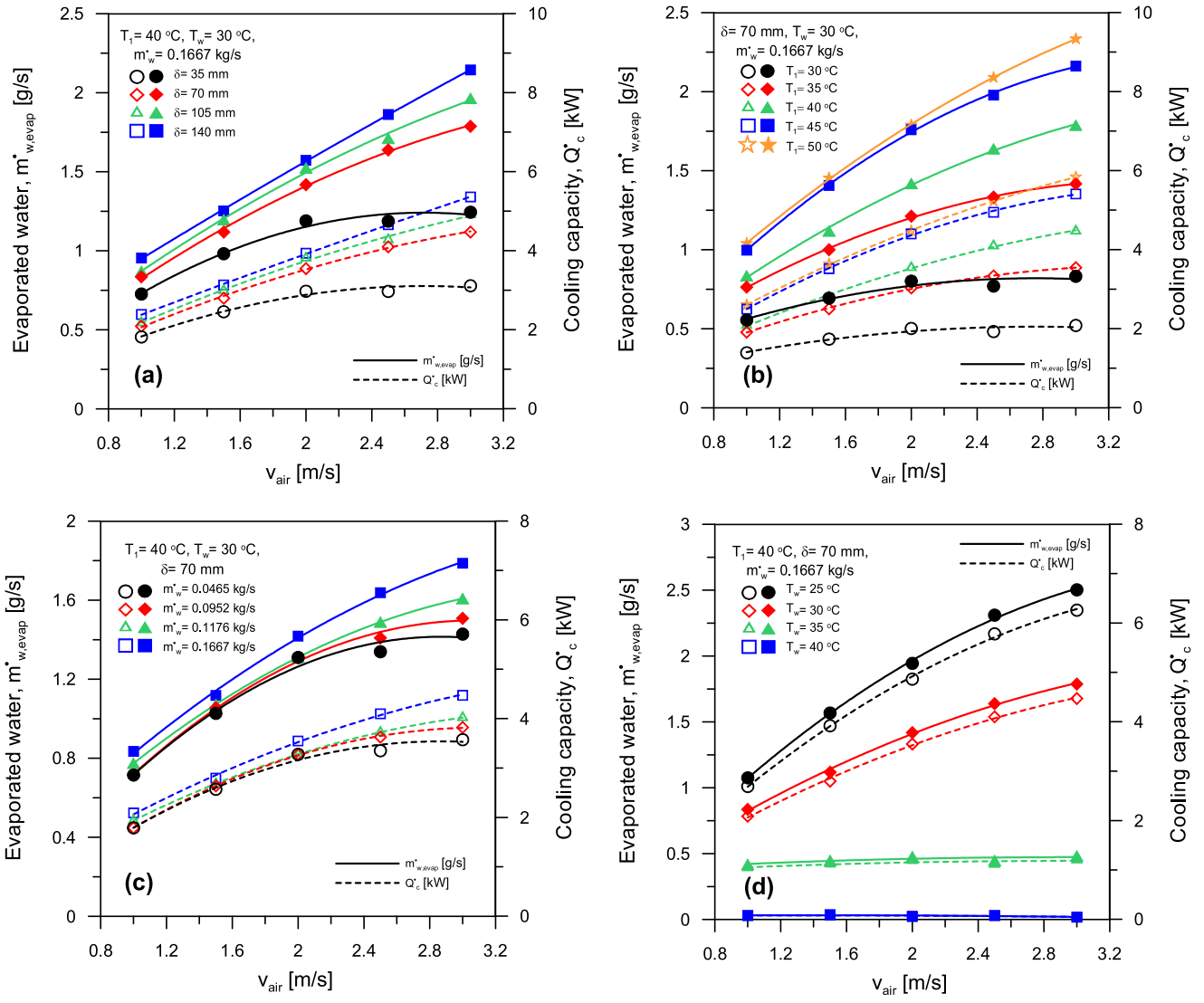

Fig. 6. Evaporated water and sensible cooling capacity of cooling pad at different: (a) pad thickness, (b) air inlet temperature, (c) humidifier-water flow rate, (d) humidifier-water temperature.

(ii) the increase of the potential difference of vapor mass transfer between the wetted cooling pad and the air due to the increase of the partial pressure differences with temperature. More evaporation means more sensible heat is extracted from the passing air which leads to higher air temperature drop. It's found at 1 m/s air velocity that the highest ΔT and Δw are 9, 12.9, 14, 17 and 18 °C and 3.7, 5.1, 5.7, 6.9 and 7.3 g_v/kg_a for inlet air temperature of 30, 35, 40, 45 and 50 °C respectively. This means that ΔT and Δw increase by 100% and 97%, respectively with the increase of the inlet air temperature from 30 °C to 50 °C.

Fig. 4-c shows the increase of the air humidity rise and temperature drop with the increase of the water flow rate. This is attributed to the increase of the air to water contact areas with the increase of water flow rate which leads to more evaporation and high humidity rise. The high humidity rise is always accompanied with high air temperature drop as the latent heat required for evaporation is extracted from the air causing reduction of its temperature. The maximum obtained ΔT and Δw at 1 m/s air velocity are 12, 12.5, 13 and 14 °C and 4.9, 5.1, 5.2 and 5.7 g_v/kg_a for water flow rates of 0.0465, 0.0952, 0.1176 and 0.1667 kg/s respectively; i.e. ΔT and Δw increases by 16.7% and 16.3%, respectively with the increase of the water flow rate from 0.0465 kg/s to 0.1667 kg/s.

Fig. 4-d shows the decrease of the air temperature drop and humidity rise across the cooling pad section with the increase of inlet water temperature. This is attributed to the increase of air temperature due to its contact with the water leading to low air temperature drop and humidity rise. It's observed that the highest ΔT and Δw obtained at 1 m/s air velocity are 18, 14, 7, and 0.5 °C and 7.4, 5.7, 2.9 and 0.2 g_v/kg_a for inlet spray water temperature of 25, 30, 35 and 40 °C respectively; i.e. ΔT and Δw deceases by 97.2% and 97.3%, respectively with the increase of the water temperature from 25 °C to 40 °C.

3.2. Saturation efficiency and pressure drop

The saturation efficiency is defined by Eq. (10) as the ratio between the actual air temperature drop across the pad section to the maximum possible temperature drop to adiabatically saturate the air. Thus, the increase of the actual air temperature drop leads to the increase of the saturation efficiency. Therefore, as shown in Fig. 4 and confirmed in Fig. 5, the air temperature drop and in consequence the saturation efficiency increases with the increase of the pad thickness, air inlet temperature, water flow rate and the decrease of air velocity and water temperature.

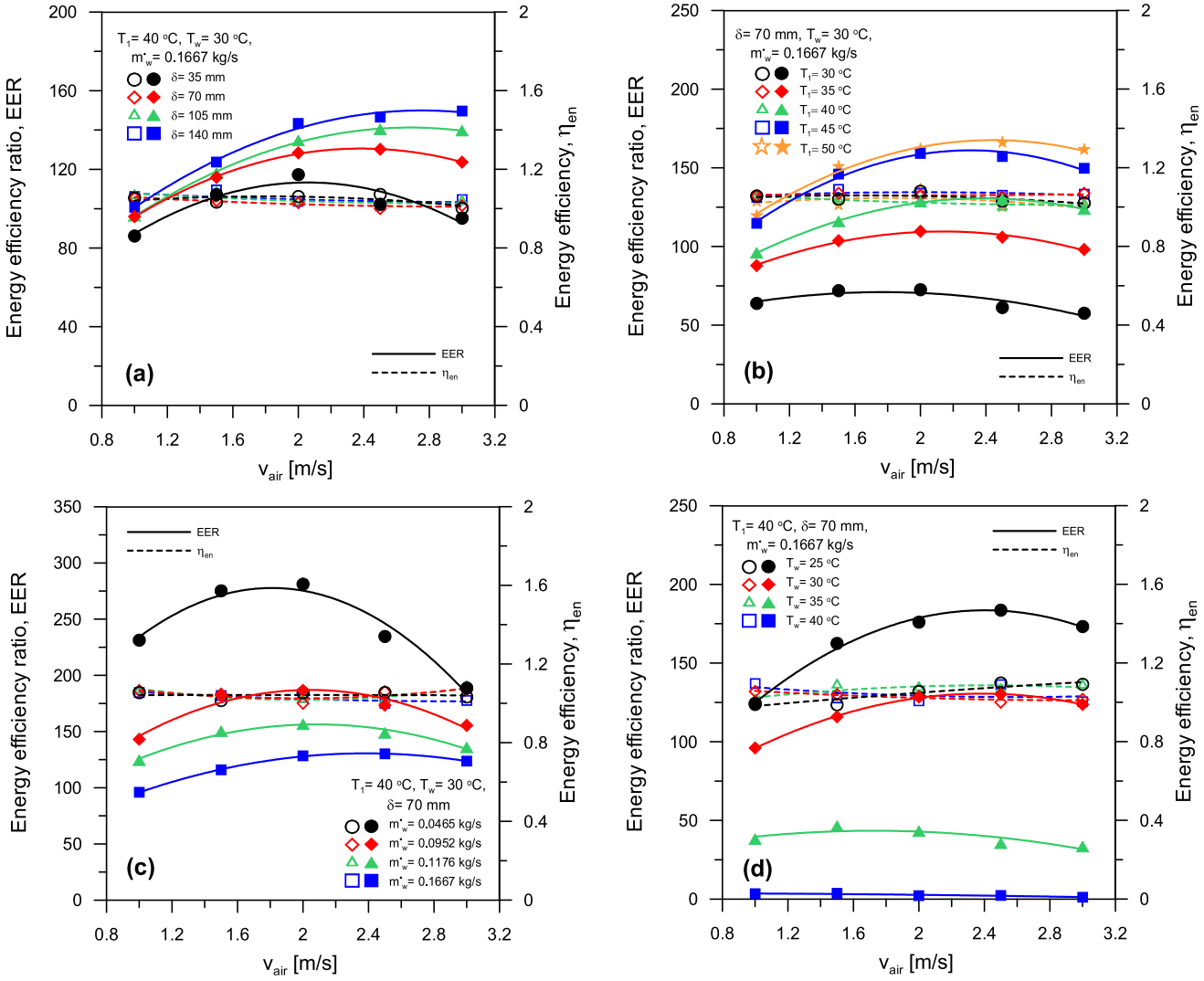

Fig. 7. Energy efficiency ratio and energy efficiency of cooling pad at different: (a) pad thickness, (b) air inlet temperature, (c) humidifier-water flow rate, (d) humidifier-water temperature.

Fig. 5-c shows the increase of the air pressure drop across the pad section with the increase of the air velocity, cooling pad thickness and water mass flow rate. However, Figs. 5-b and 5-d show that the air inlet and water temperatures don't have any effect on the pressure drop. The increase of the pressure drop with the air velocity, pad thickness and water flow rate is due to the increase of the friction between the air and the pad section, the increase of the flow resistance through the thick pad section and the decrease of the void area for air to pass in the pad section as most of the section becomes blocked with water.

Also as illustrated in Fig. 5-a, the highest saturation efficiency and the corresponding ΔP at 1 m/s air velocity are 62, 68, 73 and 77% and 4, 8, 13 and 20 Pa for 35, 70, 105 and 140 mm pad thicknesses respectively; i.e. η and ΔP increases by 26% and 400%, respectively with the increase of the pad thickness from 35 mm to 140 mm. Moreover, Fig. 5-b shows that the highest η at 1 m/s air velocity are 61, 63, 86, 71 and 73% for inlet air temperature of 30, 35, 40, 45 and 50 °C respectively and the corresponding ΔP is 8 Pa; i.e. η improves by 20% with increasing the inlet air temperature from 30 °C to 50 °C.

Furthermore, it's shown in Fig. 5-c that for 1 m/s air velocity and water flow rate of 0.0465, 0.0952, 0.1176 and 0.1667 kg/s the highest η and the corresponding ΔP are 60, 62, 64 and 68% and 4, 5, 7 and 8 Pa respectively. In other words η and ΔP increases by 14% and 100%, respectively with the increase of the water flow rate from 0.0465 kg/s to 0.1667 kg/s.

Additionally, Fig. 5-d reveals that at 1 m/s air velocity the maximum η are 83.5, 68, 34 and 2.5% for inlet water temperature of 25, 30, 35 and 40 °C respectively and the corresponding ΔP is 8 Pa.

3.3. Water evaporation rate and cooling capacity

Although Fig. 4-a shows the decrease of the air temperature drop and humidity rise with the increase of the air velocity, Fig. 6-a shows the increase of the water evaporation rate and the cooling capacity with the increase of the air velocity. Increasing the air velocity means the increase of the air mass flow rate which causes the increase of the water evaporation rate and cooling capacity (see Eqs. (2) and 16). This means that the effect of the air mass flow rate on the cooling capacity and water evaporation is more dominant than the effect of the decrease of the air temperature drop and humidity rise.

Fig. 6a-d also shows the increase of the cooling capacity and the evaporation rate with the increase of the cooling pad thickness Fig. 6-a), the increase of the air inlet temperature (Fig. 6-b), the increase of the water flow rate (Fig. 6-c) and the decrease of the water inlet temperature (Fig. 6-d). These can be attributed to the increase of the air temperature drop and humidity rise

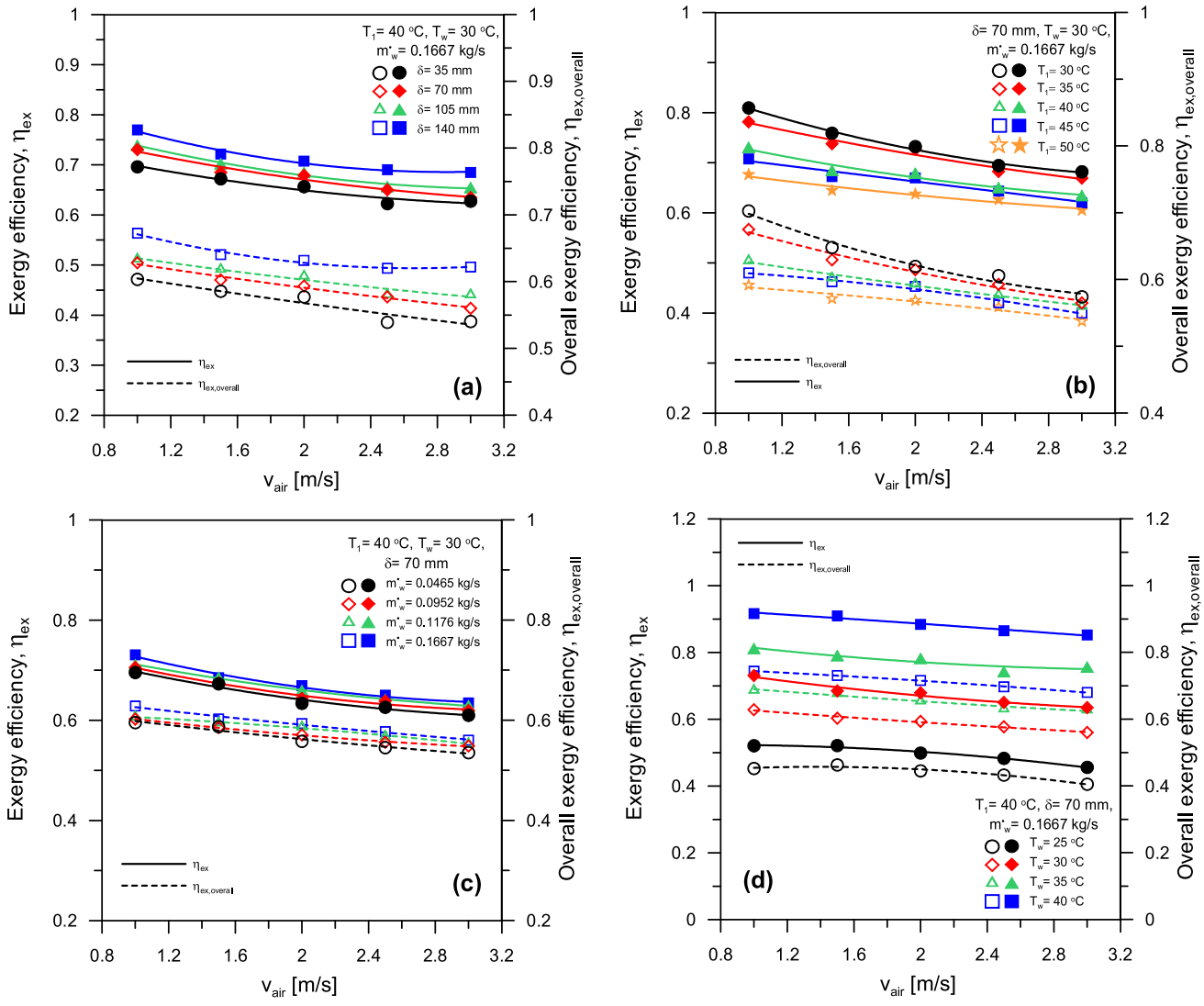

Fig. 8. Exergy and overall Exergy efficiencies of cooling pad at different: (a) pad thickness, (b) air inlet temperature, (c) humidifier-water flow rate, (d) humidifier-water temperature.

(see Eq. (2) & (16). One can predict from Fig. 6a-d that the water evaporation rate and the associated cooling capacity increases by 73% with increasing the pad thickness from 35 mm to 140 mm, by 180% with increasing the inlet air temperature from 30 °C to 50 °C, by 25% by increasing the water flow rate from 0.0465 kg/s to 0.1667 kg/s and decreases by 80% with increasing the water temperature from 25 °C to 35 °C.

3.4. Energy efficiency and energy efficiency ratio

The energy efficiency ratio (EER) is defined as the ratio between the cooling capacity and the fan and pump powers. Fig. 7 shows the effects of the different operating parameters and the pad thickness on EER and energy efficiency. As discussed in the previous section increasing the air velocity leads to the increase of the cooling capacity. At the same time increasing the air velocity causes the increase of the fan power. Fig. 7 shows the increase of EER with the increase of air velocity up to 2 m/s (highest EER) and then the EER decreases with the air velocity increase. This means that at air velocity smaller than 2 m/s the percentage of the increase of the cooling capacity with air velocity is higher that percentage of the increase of the fan power with the air velocity and vice versa at air velocity higher than 2 m/s.

Fig. 7-a and 7-c demonstrate that EER increases with the increase of the cooling pad thickness and water flow rate. This can be attributed to the increase of the cooling capacity with the increase of the pad thickness and water flow rates with percentages higher than the percentages of the increase of the fan power. As illustrated in Fig. 7-a, the highest EERs that can be obtained at 2 m/s air velocity are 117, 128, 135 and 143 for pad thicknesses of 35, 70, 105 and 140 mm respectively; i.e. EER enhances by 22% with increasing the pad thickness from 35 mm to 140 mm. While, the maximum EERs observed in Fig. 7-c at 2 m/s air velocity are 281, 187, 157 and 128 for water flow rates of 0.0465, 0.0952, 0.1176 and 0.1667 kg/s respectively; i.e. EER improves by 120% with decreasing the water flow rate from 0.1667 kg/s to 0.0465 kg/s.

Fig. 7-b and 7-d show the increase and decrease of EER with the increase of the air inlet and water temperatures, respectively. This can be attributed to the increase and the decrease of the cooling capacity with the air and water inlet temperatures, respectively. Moreover, Fig. 7-b shows that the maximum EERs are 73, 110, 128, 159, and 162 for inlet air temperature of 30, 35, 40, 45 and 50 °C respectively at 2 m/s air velocity. This means that EER increases by 122% with increasing the inlet air temperature from 30 °C to 50 °C. Whereas, Fig. 7-d reveals that the maximum EERs

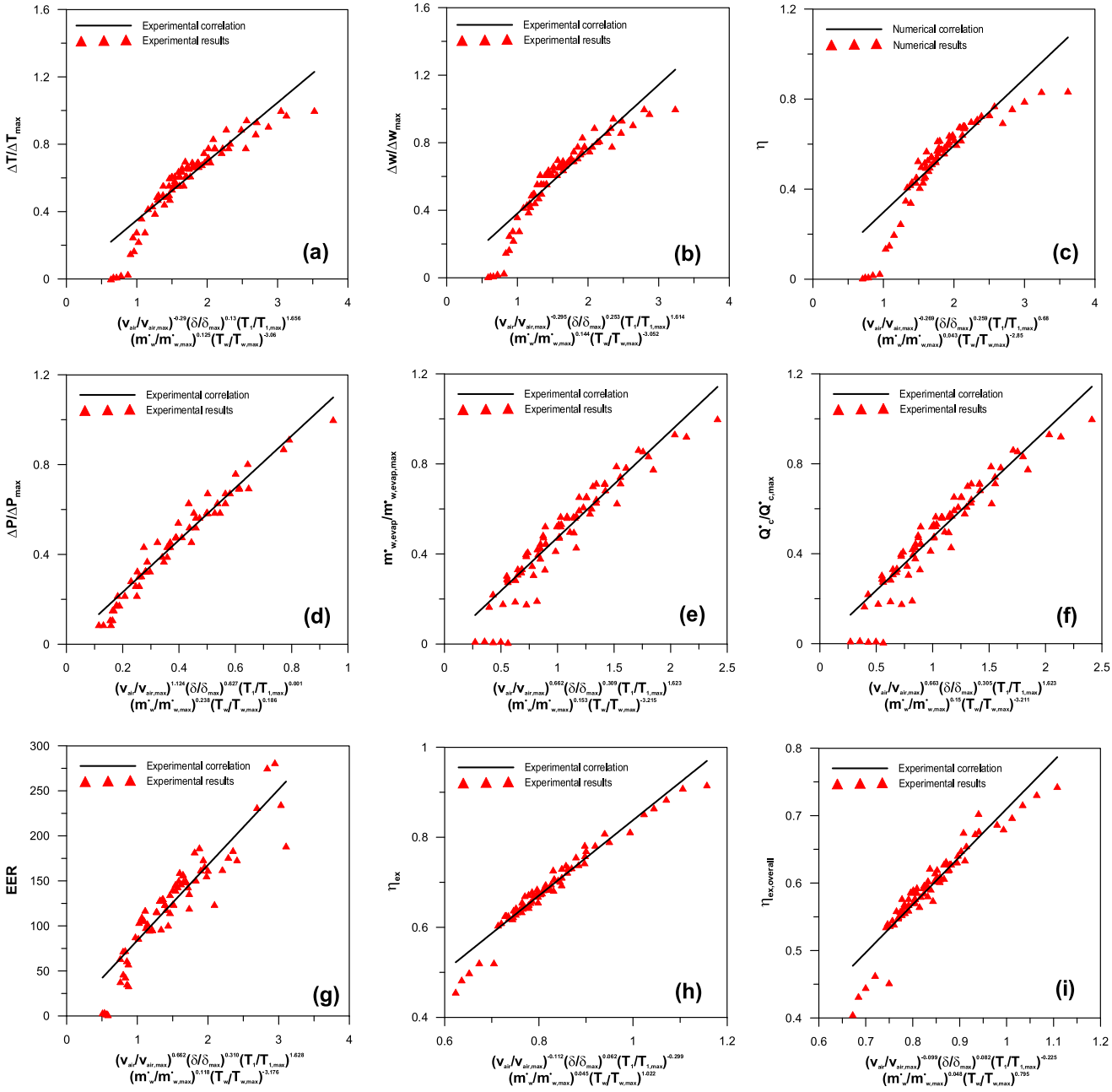

Fig. 9. Experimental correlations prediction of studied evaporative pad (bee-hive).

are 176, 128, 43 and 2 for inlet water temperature of 25, 30, 35 and 40 °C respectively at 2 m/s air velocity.

The energy efficiency, η_{en} of the cooling pad is defined as the ratio of outgoing stream energy of the air to the sum of the incoming stream energies of air and evaporated water as provided by Kanoglu et al. [25]. Theoretically, this efficiency should be 100% if the process is considered as adiabatic saturation and the test section is perfectly insulated. Fig. 7 shows that the energy efficiency can reach 105%. This proves that the actual process slightly deviates from the adiabatic saturation process especially at higher inlet water temperature and low air velocity.

3.5. Exergy efficiency and overall exergy efficiency

Fig. 8 shows the decrease of exergy efficiency η_{ex} and overall exergy efficiency $\eta_{ex,overall}$ with the increase of the air velocity for all bad thickness and operating conditions. This is due to the increase of the heat transfer rate, mass transfer rate, friction and pressure drop and the fan power with the increase of the air velocity. Increasing all of these parameters causes the increase of the exergy destruction and consequently the decrease of the exergy efficiency and the overall exergy efficiency.

Fig. 8-a demonstrates the increase of the exergy efficiency and the overall exergy efficiency with the increase of the pad thickness. Increasing the pad thickness leads to two opposite effects on η_{ex} and $\eta_{ex,overall}$ which are (i) the increase of the inlet exergy due to the increase of the water evaporation rate that causes the increase of the exergy efficiency as per Eq. (12) and (ii) the increase of the exergy destruction due to the increase of the heat transfer, mass transfer, pressure drop and the fan power in the pad section and this causes the decrease of the exergy efficiency as per Eqs.12 and 13. The effect of the increase of the inlet exergies on the exergy and the overall exergy efficiencies is more dominant than the effect of the increase of the exergy destruction with the increase of

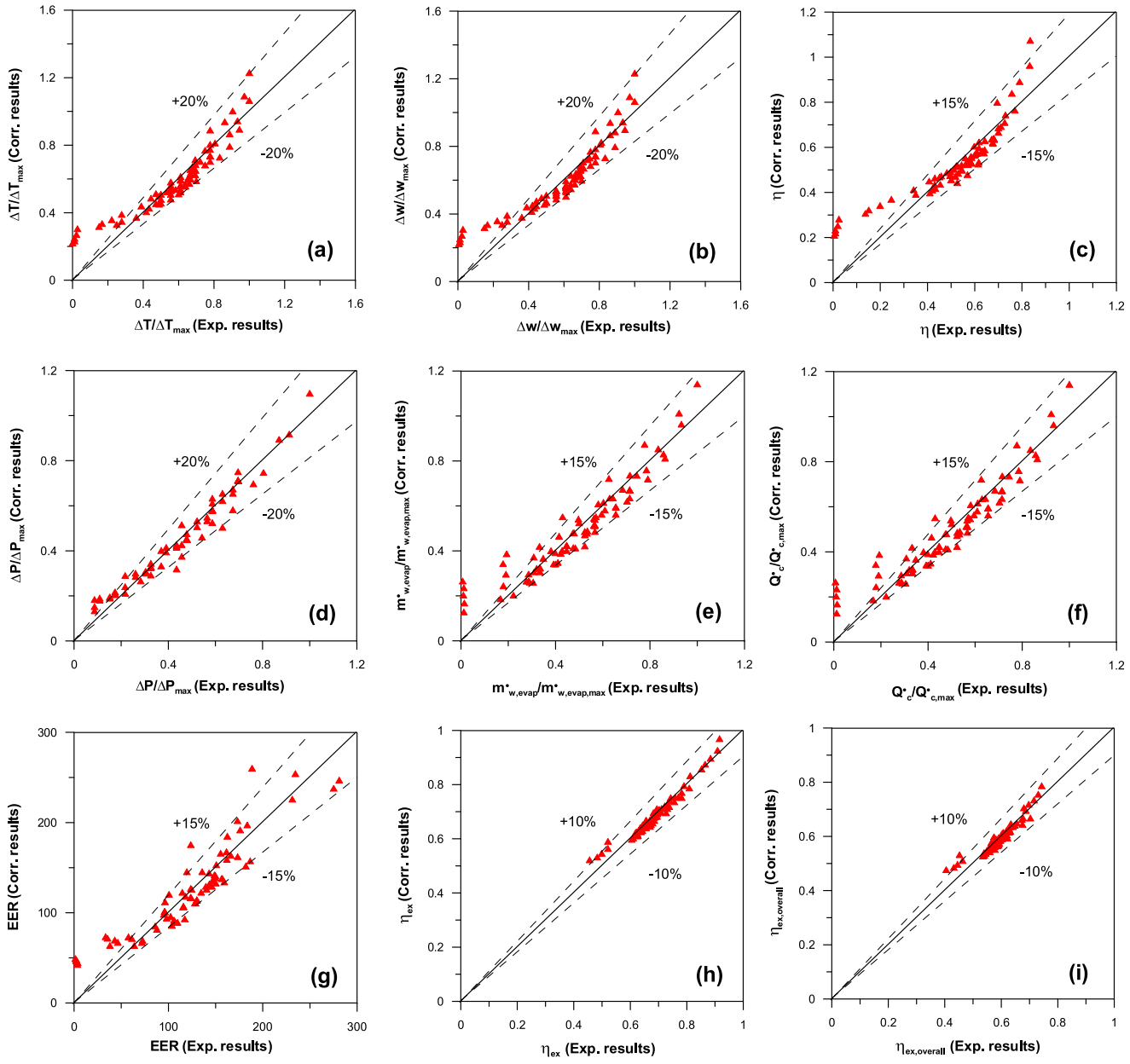

Fig. 10. Errors in experimental predicted correlations of studied evaporative pad (bee-hive).

the pad thickness (see Eqs. (12) and 13). Also as shown in Fig. 8-a, the highest values of η_{ex} and $\eta_{ex,overall}$ at 1 m/s air velocity are 70, 73, 74 and 77% and 60, 62.8, 63.4 and 67% for pad thicknesses of 35, 70, 105 and 140 mm respectively; i.e. η_{ex} and $\eta_{ex,overall}$ improves by 10% and 12%, respectively with increasing the pad thickness from 35 mm to 140 mm.

Fig. 8-b shows the decrease of the exergy efficiency and the overall exergy efficiency with the increase of the inlet air temperature. This can be attributed to the increase of the exergy destruction of the air as per Eqs. (9), 12 and 13. Fig. 8-b shows that the highest values of η_{ex} and $\eta_{ex,overall}$ at 1 m/s air velocity are 81, 78, 73, 71 and 68% and 70, 67, 63, 61 and 59% for inlet air temperatures of 30, 35, 40, 45 and 50 °C respectively; i.e. η_{ex} and $\eta_{ex,overall}$ improve by 19% and 18.6% with decreasing the inlet air temperature from 50 °C to 30 °C.

The effect of the water mass flow rate on the exergy efficiencies is shown in Fig. 8-c, where the exergy efficiencies increase with the increase of the water mass flow rates. This can be attributed to the increase of the water evaporation rate and the air temperature drop across the cooling pad and this causes the increase of the inlet exergy and the decrease of the exit exergy of the pad section, respectively. It is worth to mention that increasing the water mass flow rate increases the water pump power, air pressure drop through the pad section and both cause the increase of the exergy destruction and consequently the decrease of the exergy efficiency. This reduction of the exergy efficiency cannot overcome on the increase of the exergy efficiencies due to the increase of the water evaporation rate and the air temperature drop across the pad section. Fig. 8-c demonstrates that the maximum η_{ex} and $\eta_{ex,overall}$ at 1 m/s air velocity are 70, 70.5, 71 and 73% and 59.5, 60.2, 61 and 63% for water flow rates of 0.0465, 0.0952, 0.1176 and 0.1667 kg/s respectively; i.e. η_{ex} and $\eta_{ex,overall}$ enhances by 4.5% and 6% with increasing the spray water flow rate from 0.0465 kg/s to 0.1667 kg/s.

Fig. 8-d shows the increase of the exergy efficiencies with the increase of the inlet water temperature. This can be attributed to

Table 4
Coefficients of predicted correlations.

χ	A	B	C	D	E	F	Error
$\frac{\Delta T}{\Delta T_{max}}$	0.349	−0.29	0.13	1.656	0.125	−3.06	predicts 87% within error ±20%
$\frac{\Delta W}{\Delta W_{max}}$	0.381	−0.295	0.253	1.614	0.144	−3.052	predicts 86% within error ±20%
η	0.297	−0.269	0.259	0.68	0.043	−2.85	predicts 84% within error ±15%
$\frac{\Delta P}{\Delta P_{max}}$	1.16	1.124	0.627	0.001	0.238	0.186	predicts 88% within error ±20%
$\frac{m^{\bullet}_{w,evap}}{m^{\bullet}_{w,evap,max}}$	0.473	0.662	0.309	1.623	0.153	−3.215	predicts 85% within error ±15%
$\frac{Q^{\bullet}_{c}}{Q^{\bullet}_{c,max}}$	0.474	0.663	0.309	1.623	0.15	−3.211	predicts 84% within error ±15%
EER	3.806	0.662	0.310	1.628	0.118	−3.176	predicts 84% within error ±15%
η_{ex}	0.838	−0.112	0.062	−0.299	0.045	1.022	predicts 97% within error ±10%
$\eta_{ex,\ overall}$	0.710	−0.099	0.082	−0.225	0.048	0.795	predicts 94% within error ±10%

Table 5
Comparisons with previous different types of evaporative pads on highest saturation efficiency.

Refs.	Material type	V_{air} (m/s)	δ (mm)	$\dot{m}_w$ (kg/s)	ΔT (°C)	ΔP (Pa)	η
Al-Sulaiman [10]	Jute	2.4	50	–	–	–	0.62
Liao and Chiu [13]	Coarse fabric PVC sponge	0.5	150	0.022	–	9.8	0.86
Gunhan et al. [15]	Volcanic tuff	1.6	100	0.029	6.87	203.9	0.811
	Coarse pumice stones	1.6	100	0.029	5.99	266	0.761
	Shading net	1	150	0.029	4.42	38.1	0.513
Jain and Hindoliya [16]	Aspen fibers	1.4	–	0.045	12.7	49×10^6	0.71
	Khus fibers				11.3	14.7×10^6	0.64
	Coconut fibers				13.8	39×10^6	0.69
	Palash Fiber				15.56	29×10^6	0.81
Malli et al. [21]	cellulosic pads (7090)	1.8	150	–	–	20	0.85
Doğramacı et al. [28]	Eucalyptus fibres	0.1	20	–	9.8	–	0.71
Laknizi et al. [29]	Cellulosic pad cooling	0.5	300	–	–	6.4	0.96
Martínez et al. [1]	Plastic mesh	0.2	250	0.467	1.5	0.2	0.805
He et al. [40]	Polyvinyl Chloride (PVC)	0.5	200	0.65	–	0.9	0.5
He and Hoyano [41]	Porous Ceramic	1	–	–	4	–	0.7
Dağtekin et al. [42]	Cellulose based pad	1.25	100	0.096	5.54	–	0.84
Shrivastava et al. [43]	Coconut coir	–	70	–	13	–	0.6
Present work	Cellulose (bee-hive)	1	70	0.1667	18	8	0.84

the increase of the inlet exergy of the system with the increase of the inlet water temperature as shown in Eqs. (7) and 12. It's observed in Fig. 8-d that the highest η_{ex} and $\eta_{ex,overall}$ at 1 m/s air velocity are 52, 73, 81 and 92% and 45, 63, 69 and 74% for inlet water temperatures of 25, 30, 35 and 40 °C respectively. This means that η_{ex} and $\eta_{ex,overall}$ increase by 77% and 64%, respectively with increasing the spray water temperature from 25 °C to 40 °C.

3.6. Experimental correlations

It is worth to formulate the results in correlations to predict the performance parameters of the cooling pad in terms of the operating conditions and system size parameters. These correlations will help in the system design including the selection of the cooling pad thickness, air flow rate and water flow rate that gives the desired capacity and conditions of the system at any operating conditions. The trends of the results show that the correlations can be put in the form:

$$\chi = A\left(\frac{v_{air}}{v_{air,\max}}\right)^{B}\left(\frac{\delta}{\delta_{\max}}\right)^{C}\left(\frac{T_1}{T_{1,\max}}\right)^{D}\left(\frac{\dot{m}_w}{\dot{m}_{w,\max}}\right)^{E}\left(\frac{T_w}{T_{w,\max}}\right)^{F} \quad (19)$$

Where χ is one of the system performance parameters as given in Table 4. Eq. (19) is valid for the following ranges: 1 m/$s \le v_{air} \le$ 3 m/s, 35 mm $\le \delta \le$ 140 mm, 30 °$C \le T_1 \le$ 50 °C, 0.0465 kg/$s \le m_w$ $\le$ 0.1667 kg/s and 25 °$C \le T_w \le$ 40 °C. Where, $v_{air,max}$, δ_{max}, $T_{1,max}$, $m_{w,max}$ and $T_{w,max}$ are 3 m/s, 140 mm, 50 °C, 0.1667 kg/s and 40 °C, respectively.

In this equation and as listed in Table 4, all the performance parameters of the system and the operating conditions of the system were put in dimensionless form as a ratio of the maximum value of these parameters. Where, ΔT_{max}, Δw_{max}, ΔP_{max}, $m_{w,evap,max}$ and $Q^{\cdot}_{c,max}$ are 18 °C, 7.355 g_v/kg_a, 46 Pa, 2.5 g/s and 6.26 kW, respectively. A, B, C, D and F are constants for each performance parameter as listed in Table 4. Fig. 9 shows the techniques of predicting the equation of each performance parameters and the trend line of each equation. Fig. 10 and Table 4 also show the predicting error of the majority of the experimental data by the given equation for each parameter. The predicted equations give similar trends of the effects of the operating conditions and the system size parameters on the evaporative cooling performance that are Shown in Figs. 4-8. These correlations can be used to find the system performance parameters at any operating conditions and system design parameters.

3.7. Evaluation of the proposed cooling pad with others pads used in the literature

Based on the data obtained from literature for different cooling pad materials and types, the highest saturation efficiency and associated operating conditions of these materials and types are compared with that obtained from the current work as tabulated in Table 5. For fair comparisons of the measuring performance parameters (ΔT, ΔP and η) of the current evaporative pad with ohers pads materials in the literature, all systems must have the same operating conditions. Therefore, and according to the authors' review, some of these pad materials (e.g. Jute, Aspen fibers, Khus fibers, Coconut fibers, Eucalyptus fibres, Cellulose, etc.) are tested at closest operating conditions and pad thicknesses of the current pad type. These conditions and their references are also listed in Table 5. As shown in Table 5, at pad saturation efficiency, η (0.84), the pad used in the present work gives the highest air temperature drop ΔT (18 °C) and the lowest air pressure drop ΔP (8 Pa) as compared with other pad types. In addition, the

maximum saturation efficiency of the studied pad (cellulose paper, bee-hive) is much higher than those of other types tested in the literature [1,10,15,16,28,40,41] and [43]. Whereas, it has closer performance (i.e. approximated value of η) with Coarse fabric PVC sponge and cellulosic pads [13,21,29] and [42] that were tested at 70 mm pad thickness and higher performance (higher η) at the same operating conditions. Therefore, in general the current pad reveals higher performance parameters (η and ΔT) and lower ΔP compared with other pad types in the literature providing that the current pad (cellulose paper, bee-hive) is reliable and applicable.

4. Conclusion

The performance of cellulose paper, bee-hive evaporative cooling pad is experimentally investigated based on energy and exergy analysis for a wide range of operating conditions (air velocity, inlet air temperature, and water flow rate and water temperature) and pad thicknesses. The performance of the cooling pad was evaluated and quantified in terms of air temperature drop, air humidity rise, cooling capacity, evaporation rate, saturation efficiency, pressure drop, energy efficiency, energy efficiency ratio, exergy efficiency and overall exergy efficiency. Dimensionless experimental correlations for measuring system performance in terms of various operating conditions and system size parameters were predicted and presented within reasonable error. The findings of the present comprehensive parametric study can be summarized in the following:

- The increase of the air temperature drop and humidity rise with the increase of the pad thickness, air inlet temperature, water flow rate and the decrease of air velocity and water temperature.
- The increase of the air pressure drop across the pad section with the increase of the air velocity, cooling pad thickness and water mass flow rate. The maximum pressure drop is 46 Pa obtained at $v_{air} = 3$ m/s, $\delta =$ 140 mm, $T_1 = 40$ °C, $m_w =$ 0.1667 kg/s and $T_w =$ 30 °C.
- The increase of the saturation efficiency with the decrease of air velocity and water temperature and the increase of pad thickness, air inlet temperature and water flow rate.
- The highest saturation efficiency (η=84%) is obtained at $v_{air} = 1$ m/s, $\delta =$ 70 mm, $T_1 = 40$ °C, $m_w = 0.1667$ kg/s and $T_w = 25$ °C which can be considered as the optimum operating and design conditions. The associated air pressure drop at these conditions is 8 Pa.
- The increase of the cooling capacity and water evaporation rate with the increase of the air velocity, cooling pad thickness, air inlet temperature and water flow rate, and the decrease of the water inlet temperature. The maximum cooling capacity can be obtained from the pad is $\dot{Q}_c = 6.26$ kW at $v_{air} = 3$ m/s, $\delta =$ 70 mm, $T_1 = 40$ °C, $\dot{m}_w = 0.1667$ kg/s and $T_w = 25$ °C.
- The improvement of the energy efficiency ratio with the increase of pad thickness, air inlet temperature, and the decrease of water flow rate and water temperature. The highest energy efficiency (EER= 281) is obtained at $v_{air} = 2$ m/s, $\delta =$ 70 mm, $T_1 = 40$ °C, $m_w = 0.0465$ kg/s and $T_w = 30$ °C.
- The enhancement of the exergy and overall exergy efficiencies with the decrease of air velocity and air inlet temperature and the increase of pad thickness, water flow rate, and water temperature. The maximum exergy and overall exergy efficiencies are $\eta_{ex} = 92\%$ and $\eta_{ex,overall} =$ 74% and are obtained at $v_{air} = 1$ m/s, $\delta =$ 70 mm, $T_1 = 40$ °C, $m_w = 0.1667$ kg/s and $T_w = 40$ °C.

Declaration of Competing Interest

The authors declare that they have no known competing financial interests or personal relationships that could have appeared to influence the work reported in this paper.

References

[1] P. Martínez, J. Ruiz, P.J. Martínez, A.S. Kaiser, M. Lucas, Experimental study of the energy and exergy performance of a plastic mesh evaporative pad used in air conditioning applications, Appl. Therm. Eng. 138 (2018) 675–685.
[2] A. Fouda, Z. Melikyan, A simplified model for analysis of heat and mass transfer in a direct evaporative cooler, Appl. Therm. Eng. 31 (2011) 932–936.
[3] Deepak Bishoyi, K. Sudhakar, Experimental performance of a direct evaporative cooler in composite climate of india, Energy Build. 153 (2017) 190–200.
[4] W.Y. Saman, A. Percy, P. Sardelis, J. McNab, A comparison between a conventional heat pump system and one incorporating heat recovery/evaporative cooling, Proc International Symposium on Energy, Environment and Economics, 1995.
[5] F.W. Yu, K.T. Chan, Improved condenser design and condenser-fan operation for air-cooled chillers, Appl. Energy 83 (6) (2006) 628–648.
[6] Xiaoli Hao, Cangzhou Zhu, Yaolin Lin, Haiqiao Wang, Guoqiang Zhang, Youming Chen, Optimizing the pad thickness of evaporative air-cooled chiller for maximum energy saving, Energy Build. 61 (2013) 146–152.
[7] E. Hajidavalloo, H. Eghtedari, Performance improvement of air-cooled refrigeration system by using evaporatively cooled air condenser, Int. J. Refrig 33 (5) (2010) 982–988.
[8] Adel A. Eidan, Kareem J. Alwan, Assaad AlSahlani, Mohamed Alfahham, Enhancement of the performance characteristics for Air- Conditioning System by using direct evaporative cooling in hot cilmates, in: 9th International Conference on Applied Energy, ICAE2017, 21-24 August 2017, 142, Cardiff, UK, 2017, pp. 3998–4003. Energy Procedia.
[9] T. Wang, C. Sheng, A.G.A. Nnanna, Experimental investigation of air conditioning system using evaporative cooling condenser, Energy Build 81 (2014) 435–443.
[10] F. Al-Sulaiman, Evaluation of the performance of local fibers in evaporative cooling, Energy Convers. Manage 43 (2002) 2267–2273.
[11] R.W. Koca, W.C. Hughes, L.L. Christianson, Evaporative cooling pads: test procedure and evaluation, Appl. Eng. Agric 7 (4) (1991) 485–490.
[12] Igor Kovačević, Maarten Sourbron, The numerical model for direct evaporative cooler, Appl. Therm. Eng. 113 (2017) 8–19.
[13] C.M. Liao, K.H. Chiu, Wind tunnel modeling the system performance of alternative evaporative cooling pads in Taiwan region, Build. Environ 37 (2) (2002) 177–187.
[14] R. Rawangkul, J. Khedari, J. Hirunlabh, B Zeghmati, Performance analysis of a new sustainable evaporative cooling pad made from coconut coir, Int. J. Sustain. Eng. 1 (2) (2008) 117–131.
[15] T. Gunhan, V. Demir, A.K. Yagcioglu, Evaluation of the suitability of some local materials as cooling pads, Biosyst. Eng 96 (3) (2007) 369–377.
[16] J.K. Jain, D.A. Hindoliya, Experimental performance of new evaporative cooling pad materials, Sust. Cities Soc. 1 (2011) 252–256.
[17] A. Beshkani, R. Hosseini, Numerical modeling of rigid media evaporative cooler, Appl. Therm. Eng 26 (5–6) (2006) 636–643.
[18] Y.J. Dai, K. Sumathy, Theoretical study on a cross-flow direct evaporative cooler using honeycomb papers as packing material, Appl. Therm. Eng. 22 (2002) 1417–1430.
[19] J.M. Wu, X. Huang, H. Zhang, Numerical investigation on the heat and mass transfer in a direct evaporative cooler, Appl. Therm. Eng. 29 (1) (2009) 195–201.
[20] J.M. Wu, X. Huang, H. Zhang, Theoretical analysis on heat and mass transfer in a direct evaporative cooler, Appl. Therm. Eng. 29 (5–6) (2009) 980–984.
[21] A. Malli, H.R. Seyf, M. Layeghi, S. Sharifian, H. Behravesh, Investigating the performance of cellulosic evaporative cooling pads, Energy Convers. Manage. 52 (7) (2011) 2598–2603.
[22] Amrat Kumar Dhamneya, S.P.S. Rajput, Alok Singh, Thermodynamic performance analysis of direct evaporative cooling system for increased heat and mass transfer area, Ain Shams Eng. J. 9 (2018) 2951–2960.
[23] A. Fouda, S.A. Nada, H.F. E.lattar, S. Rubaiee, A. Al-Zahrani, Performance analysis of proposed solar hdh water desalination systems for hot and humid climate cities, Appl. Therm. Eng. 144 (2018) 81–95.
[24] A. Fouda, S.A. Nada, H.F. Elattar, An integrated A/C and HDH water desalination system assisted by solar energy: transient analysis and economical study, Appl. Therm. Eng. 108 (2016) 1320–1335.
[25] H.F. Elattar, A. Fouda, S.A. Nada, Performance investigation of a novel solar hybrid air conditioning and humidification–dehumidification water desalination system, Desalination 382 (2016) 28–42.
[26] S.A. Nada, H.F. Elattar, A. Fouda, Performance analysis of proposed hybrid air conditioning and humidification–dehumidification systems for energy saving and water production in hot and dry climatic regions, Energy Conversion Manage. 96 (2015) 208–227.
[27] S.A. Nada, H.F. Elattar, A. Fouda, Experimental study for hybrid humidification–dehumidification water desalination and air conditioning system, Desalination 363 (2015) 112–125.

[28] Pervin Abohorlu Doğramacı, Saffa Riffat, Guohui Gan, Devrim Aydın, Experimental study of the potential of eucalyptus fibres for evaporative cooling, Renew. Energy 131 (2019) 250–260.
[29] Azzeddine Laknizi, Mustapha Mahdaoui, Abdelatif Ben Abdellah, Kamal Anoune, Mohamed Bakhouya, Hassan Ezbakhe, Performance analysis and optimal parameters of a direct evaporative pad cooling system under the climate conditions of morocco, Case Studies in Therm. Eng. 13 (2019) 100362.
[30] M. Kanoglu, I. Dincer, M.A. Rosen, Exergy analysis of psychrometric processes for HVAC&R applications, ASHRAE Trans. 113 part 2 (2007) 172–180.
[31] J.C. Santos, G.D.T. Barros, J.M. Gurgel, F. Marcondes, Energy and exergy analysis applied to the evaporative cooling process in air washers, Int. J. Refrig 36 (3) (2013) 1154–1161.
[32] TABREED, Cooling Cell Pads, (accessed on 03.05.2019). http://www.tabreed coolingpads.com.
[33] A. Franco, D.L. Valera, A. Madueño, A. Peña, Influence of water and air flow on the performance of cellulose evaporative cooling pads used in mediterranean greenhouses, Trans. ASABE 53 (2) (2010) 565–576.
[34] I. Dincer, M.A. Rosen, Exergy: energy, Environment and Sustainable Development, 2nd ed., Elsevier Science, 2012 ISBN: 9780080970899.
[35] M.J. Moran, H.N. Shapiro, D.D. Boettner, M.B. Bailey, Fundamentals of Engineering Thermodynamics, 8th ed., John Wiley/& Sons, Inc., Hoboken, New Jersey, 2014.
[36] ASHRAE standard ANSI/ASHRAE 133-2001, method of testing direct evaporative air coolers, 2001, p. 24.
[37] C. Lertsatitthanakorn, et al., Field experiment and economic evaluation of an evaporative cooling systemin a silkworm rearing house, Silsoe Res. Instit. (2006).
[38] R.J. Moffat, Describing the uncertainties in experimental results, Exp. Therm. Fluid Sci 1 (1) (1988) 3–17.
[39] J.R. Taylor, An Introduction to Error Analysis: The Study of Uncertainties in Physical Measurements, 2nd ed., University Science Books, Sausalito, CA, 1997.
[40] S. He, Z. Guan, H. Gurgenci, K. Hooman, Y. Lu, A.M. Alkhedhair, Experimental study of film media used for evaporative pre-cooling of air, Energy Convers. Manage 87 (2014) 874–884.
[41] J. He, A. Hoyano, Experimental study of cooling effects of a passive evaporative cooling wall constructed of porous ceramics with high water soaking-up ability, Build. Environ 45 (2011) 461–472.
[42] M. Dagtekin, C. Karaca, Y. Yildiz, A. Bas¸ çetinçelik, Ö. Paydak, The effects of air velocity on the performance of pad evaporative cooling systems, Afr. J. Agric. Res 6 (7) (2011) 1813–1822.
[43] K. Shrivastava, D. Deshmukh, M.V. Rawlani, Experimental analysis of coconut coir pad evaporative cooler, Int. J. Innov. Res. Sci., Eng. Technol 3 (2014) 8346–8351.